

## **Electrophysiological properties of anion exchangers in the luminal membrane of guinea pig pancreatic duct cells**

N. Andharia • M. Hayashi • H. Matsuda

### **Author affiliation:**

N. Andharia • M. Hayashi • H. Matsuda

Department of Physiology, Kansai Medical University, 2-5-1 Shinmachi, Hirakata 573-1010, Japan

### **Corresponding author:**

M. Hayashi

e-mail: [REDACTED]

phone: [REDACTED]

fax: [REDACTED]

### **Acknowledgments:**

This work was supported by the research grant D2 from Kansai Medical University, the Pancreas Research Foundation of Japan, and Japan Society for the Promotion of Science KAKENHI (24790226). N. Andharia was supported by the Rotary Yoneyama Memorial Foundation.

### **Compliance with ethical standards:**

### **Conflict of interest:**

The authors declare that they have no conflict of interest.

### **Ethical approval:**

All procedures performed in studies involving animals were in accordance with the ethical standards of the institution or practice at which the studies were conducted.

## Abstract

The pancreatic duct epithelium secretes the  $\text{HCO}_3^-$ -rich pancreatic juice. The  $\text{HCO}_3^-$  transport across the luminal membrane has been proposed to be mediated by SLC26A  $\text{Cl}^-$ - $\text{HCO}_3^-$  exchangers. To examine the electrophysiological properties of  $\text{Cl}^-$ - $\text{HCO}_3^-$  exchangers, we directly measured  $\text{HCO}_3^-$  conductance in the luminal membrane of the interlobular pancreatic duct cells from guinea pigs using an inside-out patch-clamp technique. Intracellular  $\text{HCO}_3^-$  increased the  $\text{HCO}_3^-$  conductance with a half-maximal effective concentration value of approximately 30 mM. The selectivity sequence based on permeability ratios was  $\text{SCN}^-$  (1.4) >  $\text{Cl}^-$  (1.2) = gluconate (1.1) =  $\Gamma^-$  (1.1) =  $\text{HCO}_3^-$  (1.0) > methanesulfonate (0.6). The sequence of the relative conductance was  $\text{HCO}_3^-$  (1.0) >  $\text{SCN}^-$  (0.7) =  $\Gamma^-$  (0.7) >  $\text{Cl}^-$  (0.5) = gluconate (0.4) > methanesulfonate (0.2). The current dependent on intracellular  $\text{HCO}_3^-$  was reduced by replacement of extracellular  $\text{Cl}^-$  with gluconate or by H<sub>2</sub>DIDS, an inhibitor of  $\text{Cl}^-$ - $\text{HCO}_3^-$  exchangers. RT-PCR analysis revealed that the interlobular and main ducts expressed all SLC26A family members except *Slc26a5* and *Slc26a8*. SLC26A1, SLC26A4, SLC26A6, and SLC26A10 were found to be localized to the luminal membrane of the guinea pig pancreatic duct by immunohistochemistry. These results demonstrate that these SLC26A  $\text{Cl}^-$ - $\text{HCO}_3^-$  exchangers may mediate the electrogenic  $\text{HCO}_3^-$  transport through the luminal membrane and may be involved in pancreatic secretion in guinea pig ducts.

## Keywords

bicarbonate; duct; exchanger; pancreas; patch-clamp; SLC26

## Introduction

The pancreas plays a pivotal role in digestion. Pancreatic acini secrete digestive enzyme-rich neutral fluid that is not dependent on the presence of the  $\text{CO}_2/\text{HCO}_3^-$ -buffer system. However, ducts secrete a  $\text{HCO}_3^-$ -rich fluid, which is dependent on the presence of  $\text{CO}_2/\text{HCO}_3^-$ -buffer, and that neutralizes acid chyme in the duodenum [33]. The generally accepted model for  $\text{HCO}_3^-$  transport involves  $\text{Cl}^-$ - $\text{HCO}_3^-$  exchangers that operate in parallel with cAMP-activated  $\text{Cl}^-$  channels [cystic fibrosis transmembrane conductance regulator (CFTR)] and  $\text{Ca}^{2+}$ -activated  $\text{Cl}^-$  channels, such as TMEM16A/ANO1, on the luminal membranes of duct cells [42, 49]. TMEM16A/ANO1 is also found specifically in the apical membranes of the acinar cells and is the critical channel for the control of acinar fluid secretion [32]. In addition,  $\text{H}^+$ - $\text{K}^+$ -pumps and  $\text{K}^+$  channels are expressed on the luminal membrane of pancreatic ducts [12, 28, 45].  $\text{K}^+$  channels are important for setting the resting membrane potential and for providing the driving force for anion transport, and may provide the transport partners for  $\text{H}^+$ - $\text{K}^+$ -pumps [11].

Electrophysiological studies have found a luminal  $\text{Cl}^-$  conductance in rat pancreatic ducts [6, 27]. Single-channel recordings revealed small-conductance  $\text{Cl}^-$  channels on the luminal membrane of duct cells, which were identified as CFTR  $\text{Cl}^-$  channels [6, 8]. The  $\text{HCO}_3^-/\text{Cl}^-$  permeability ratios of CFTR  $\text{Cl}^-$  channels have been reported as 0.1 to 0.4 [8, 30] and demonstrated to be increased to 1.0 by reducing the intracellular  $\text{Cl}^-$  concentration in pancreatic duct cells [31]. Measurement of intracellular pH and membrane potential of guinea pig duct cells suggested that CFTR  $\text{Cl}^-$  channels provide

a significant pathway for  $\text{HCO}_3^-$  secretion [17].

Another pathway for  $\text{HCO}_3^-$  secretion across the luminal membrane is the  $\text{Cl}^-$ - $\text{HCO}_3^-$  exchanger, which has been identified as solute carrier family 26 member A6 (SLC26A6) [14, 20, 47]. SLC26A6 has been found to be electrogenic with a  $1\text{Cl}^-/2\text{HCO}_3^-$  exchange stoichiometry in *Xenopus* oocytes and HEK 293 cells [19, 38]. Consistently with this, deletion of *Slc26a6* altered the overall stoichiometry of apical  $\text{Cl}^-$ - $\text{HCO}_3^-$  exchange in native mouse interlobular ducts, suggesting the upregulation of a  $\text{Cl}^-$ - $\text{HCO}_3^-$  exchanger with different stoichiometry [41]. Previous studies have demonstrated a functional coupling between CFTR  $\text{Cl}^-$  channels and  $\text{Cl}^-$ - $\text{HCO}_3^-$  exchange activity in isolated pancreatic interlobular ducts [15, 44]. Furthermore, a computational model suggested that the  $\text{HCO}_3^-/\text{Cl}^-$  permeability ratio of apical  $\text{Cl}^-$  channels of 0.4 was able to support  $\text{HCO}_3^-$  secretion [50]. However, few studies have examined the electrophysiological properties and regulation of  $\text{HCO}_3^-$  conductance across the luminal membrane of native pancreatic duct cells.

The aim of the present study was to identify  $\text{HCO}_3^-$  conductance that is important for pancreatic secretion. For this purpose, we directly measured  $\text{HCO}_3^-$  currents through the luminal membrane of guinea pig pancreatic duct cells using the patch clamp method in the inside-out configuration. We demonstrated that the inward conductance is dependent on intracellular  $\text{HCO}_3^-$  and extracellular  $\text{Cl}^-$ , and is blocked by  $\text{H}_2\text{DIDS}$ , an inhibitor of anion transporters, and thus conclude that such inward conductance is carried out via anion exchangers on the luminal membrane. Furthermore, we report the expression and localization of the SLC26A family in the interlobular and main

pancreatic duct using molecular biological and immunohistochemical analyses.

## Methods

### *Preparation of pancreatic duct cells from guinea pigs*

Female Hartley guinea pigs (240–450 g,  $n = 35$ ) were sacrificed by carbon dioxide stunning in accordance with protocols approved by the Animal Experimentation Committee, Kansai Medical University. Pancreatic ducts were isolated by enzymatic digestion and microdissection from the pancreas as previously described [10]. The pancreas was removed, and digested with collagenase (Type IV, 124 U/ml; Worthington) and trypsin inhibitor (0.01%; Sigma) in Tyrode solution at 37°C for 1 hour with vigorous shaking. Tyrode solution contained the following (in mM): 140 NaCl, 0.33 NaH<sub>2</sub>PO<sub>4</sub>, 5.4 KCl, 1.8 CaCl<sub>2</sub>, 0.5 MgCl<sub>2</sub>, 5 HEPES, and 5.5 D-glucose; pH was adjusted to 7.4 with NaOH. Interlobular and intralobular ducts (outside diameter of 30–60 μm) were microdissected under a stereomicroscope. The ducts were washed in Tyrode solution and then placed on coverslips pretreated with Cell-Tak (BD Biosciences). In order to allow patch-clamp access to the luminal membranes of the lining of epithelial cells, the ducts were split open by patch pipettes.

### *Patch-clamp recording*

Standard patch-clamp techniques were used. Patch pipettes, pulled from capillaries of hard borosilicate glass (G-1.5; Narishige), had a resistance of 5–7 MΩ when filled with a standard *N*-methyl-D-glucamine (NMDG)-Cl solution. The standard NMDG-Cl

solution contained the following (in mM): 130 NMDG, 130 HCl, 5 EGTA, and 10 HEPES; pH was adjusted to 7.4 with NMDG. The stripped duct was bathed in a standard bicarbonate solution consisting of (in mM): 115 NaCl, 5 KCl, 1 CaCl<sub>2</sub>, 1 MgCl<sub>2</sub>, 25 NaHCO<sub>3</sub>, 10 HEPES (pH 7.4, adjusted with NaOH), and 5.5 D-glucose. The standard bicarbonate solution was equilibrated with 5% CO<sub>2</sub> in O<sub>2</sub>. The membrane potential was corrected for the liquid junction potential at the tip of the patch pipette in the bathing solution, and for that at the tip of the indifferent reference electrode filled with Tyrode solution and placed in the bath. Experiments were conducted at 23–30°C. After the inside-out configuration was established, the solution in the perfusion chamber was switched to control bicarbonate solution. The control bicarbonate solution contained the following (in mM): 130 KHCO<sub>3</sub>, 5 EGTA, and 10 HEPES; pH was 7.8–8.0 after adding bicarbonate. A standard chloride solution contained the following (in mM): 130 KCl, 5 EGTA, and 10 HEPES; pH was adjusted to 7.8 with KOH. To record the HCO<sub>3</sub><sup>-</sup> selective conductance, the control bicarbonate solution was mixed with the standard chloride solution to make different concentrations (0, 16, 33, 65, and 130 mM) of HCO<sub>3</sub><sup>-</sup> around pH 7.8–8.0. To test the anion selectivity, KHCO<sub>3</sub> in the control bicarbonate solution was replaced with anions such as KCl, K-gluconate, K-methanesulfonate, K-thiocyanate, or KI at pH 7.8. The concentration of free Ca<sup>2+</sup> was calculated using the MaxChelator computer program. 4,4'-diisothiocyano-2,2'-dihydrostilbenedisulfonic acid disodium salt (H<sub>2</sub>DIDS; Toronto Research Chemicals) was directly dissolved at 0.5 mM in control bicarbonate solution. 4-[[4-oxo-2-thioxo-3-[3-trifluoromethyl)phenyl]-5-thiazolidinylidene]methyl]benzoic acid (CFTRinh-172; Santa Cruz Biotechnology) and 2-Methyl-8-(phenylmethoxy)imidazo[1,2-a]pyridine-3-acetonitrile (Sch28080; Santa

Cruz Biotechnology) were dissolved in DMSO at a 1000-fold concentration for application. The current was recorded in the inside-out configuration using the EPC 800 patch-clamp amplifier (HEKA). The amplifier was driven by Clampex 9 (Axon) in order to allow the delivery of a voltage-ramp protocol with concomitant digitization of the current. The membrane potential was generally held at 0 mV, and the command voltage was varied from  $-80$  to  $+80$  mV over a duration of 800 ms every 10 s.

#### *RT-PCR analysis*

RNA was extracted from the interlobular (outside diameter of 50–150  $\mu\text{m}$ ) and main ducts (outside diameter of around 500  $\mu\text{m}$ ) from three independent guinea pigs using the RNeasy Plus Micro kit with DNase I (Qiagen). RT-PCR analysis was performed using the OneStep RT-PCR kit (Qiagen) with primers designed to recognize different types of transporters (Table 1). For the negative control of reverse transcription, we used *Taq* DNA Polymerase (Promega). The amplification parameters used were as follows: one cycle at  $50^{\circ}\text{C}$  for 30 min and one cycle at  $95^{\circ}\text{C}$  for 15 min, followed by 40 cycles at  $94^{\circ}\text{C}$  for 30 s,  $57^{\circ}\text{C}$  for 30 s,  $72^{\circ}\text{C}$  for 30 s, and one cycle at  $72^{\circ}\text{C}$  for 10 min. The transcripts were subsequently verified by agarose gel electrophoresis.

#### *Immunolocalization*

Immunolocalization was performed on the guinea pig pancreas. The pancreas was obtained from female Hartley guinea pigs ( $n = 3$ ) in accordance with protocols approved by the Animal Experimentation Committee, Kansai Medical University. The guinea pigs were anesthetized with isoflurane and a mixture of medetomidine (0.5 mg/kg body weight), midazolam (5.0 mg/kg b.w.), and butorphanol (2.5 mg/kg b.w.), and perfused

transcardially with 4% paraformaldehyde. The pancreas was fixed with 4% paraformaldehyde in PBS for 24 hours, embedded in paraffin, and sectioned. Detailed methods for immunohistochemistry were described previously [10]. Briefly, autofluorescence was blocked by 0.1 M Tris-glycine. Non-specific binding was blocked with 2% normal donkey serum in PBS. Preparations were subsequently incubated with primary antibodies for SLC26A1, SLC26A3, SLC26A4, SLC26A6, or SLC26A10 (Table 2), along with Ezrin (1:400 to 1:800, clone 3C12, MS-661; Lab Vision) and PECAM-1 (platelet endothelial cell adhesion molecule-1, 1:800, sc-1506; Santa Cruz Biotechnology) in immunoreaction enhancer solution (Can Get Signal immunostain; Toyobo) overnight at 4°C. Secondary antibodies conjugated to Alexa488 (SLC26A), Alexa568 (Ezrin), or Alexa647 (PECAM-1) (1:400; Molecular Probes) were added for 1 hour. For the negative control, the primary antibodies were pre-absorbed with corresponding antigens for SLC26A1 (APrEST81987; Atlas), SLC26A10 (APrEST84901), SLC26A4 (synthesized peptide; Eurofins Genomics), or SLC26A6 (synthesized peptide) for 30 min at room temperature. In the controls, the primary antibodies were omitted and scanning was performed using the same settings. Nuclei were stained with 4',6-diamidino-2-phenylindole (DAPI) at 1 µg/ml. Fluorescence was observed with a confocal laser scanning microscope (LSM510 META; Carl Zeiss).

#### *Western immunoblotting*

The pancreatic duct was dissected from three independent guinea pigs as described above. The ducts were washed with cold PBS, treated with trichloroacetic acid (10%) on ice for 30 min, and then centrifuged. The pellet was solubilized in lysis buffer

containing urea (9 M), Triton X-100 (2%), dithiothreitol (1%), and lithium dodecyl sulfate (2%). The samples (30  $\mu$ g/lane protein) were fractionated on SDS polyacrylamide gel (7.5%), electroblotted to PVDF membranes (Merck Millipore), blocked with skim milk (1%), and reacted with anti-SLC26A4, anti-SLC26A6, or anti-SLC26A10 antibodies (Table 2). For anti-SLC26A1, we used signal enhancer Hikari solution (Nacalai Tesque, Kyoto, Japan). The reaction was visualized with a secondary antibody labeled with alkaline phosphatase (Promega).

### *Statistics*

Data are shown as means  $\pm$  SEM. A one-way analysis of variance (ANOVA) or Student's paired *t*-test was applied, and  $P < 0.05$  was considered significant. Data were analyzed in Igor or Microsoft Excel.

## **Results**

### *Bicarbonate conductance through the luminal membrane of the interlobular pancreatic duct cells*

We recorded macroscopic currents from excised inside-out patches from the luminal membrane of the interlobular pancreatic duct cells of guinea pigs under unstimulated conditions. Figure 1a shows the macroscopic current–voltage (*I*–*V*) relationships in the presence of intracellular  $\text{HCO}_3^-$  at different concentrations (0, 16, 33, 65, and 130 mM). As we used the standard NMDG-Cl pipette solution and the bathing solution containing  $\text{KHCO}_3$ , the inward current was due to  $\text{HCO}_3^-$  efflux through the luminal membrane.

The inward conductance determined from the linear section of the  $I$ - $V$  relationships (from  $-80$  to  $-60$  mV) increased with intracellular  $\text{HCO}_3^-$  concentration (Fig. 1a). The linear plot of conductance with the  $\text{HCO}_3^-$  concentration had a sigmoid relationship (Fig. 1b). The half-maximal effective concentration ( $K_d$ ) value for the effects of  $\text{HCO}_3^-$  and Hill coefficient were  $31.5 \pm 5.1$  mM and  $3.5 \pm 0.4$  ( $n = 5$ ), respectively. We also measured inward  $\text{HCO}_3^-$  currents in the bathing solution containing 130 mM  $\text{NaHCO}_3$ . The inward conductance increased to  $2.04 \pm 0.95$  nS in  $\text{NaHCO}_3$  from  $0.34 \pm 0.08$  nS in  $\text{NaCl}$  (data not shown;  $n = 13$ ). Thus, there was a minor contribution of  $\text{K}^+$  conductance under unstimulated conditions.

#### *Ion selectivity of the bicarbonate conductance*

Ion selectivity of the bicarbonate conductance was examined by replacing 130 mM  $\text{HCO}_3^-$  in the intracellular bathing solution with other monovalent anions. Figure 2 shows macroscopic  $I$ - $V$  relations recorded in the inside-out configuration with the standard NMDG-Cl pipette solution. In experiments where  $\text{HCO}_3^-$  in the bath was replaced with  $\text{Cl}^-$  or gluconate ( $\text{glc}^-$ ), the reversal potential did not change, but inward conductance significantly decreased from  $1.30 \pm 0.09$  nS in  $\text{HCO}_3^-$  to  $0.64 \pm 0.13$  nS in  $\text{Cl}^-$  (Figs. 2a and 3b (right);  $n = 5$ ) and from  $1.69 \pm 0.08$  nS in  $\text{HCO}_3^-$  to  $0.72 \pm 0.14$  nS in  $\text{glc}^-$  (Fig. 2b;  $n = 5$ ). Replacement of  $\text{HCO}_3^-$  with methanesulfonate ( $\text{MES}^-$ ) shifted the reversal potential in a negative direction, indicating it was less permeable than  $\text{HCO}_3^-$ , and the inward conductance significantly decreased from  $2.56 \pm 0.73$  nS in  $\text{HCO}_3^-$  to  $0.73 \pm 0.36$  nS in  $\text{MES}^-$  (Fig. 2c;  $n = 6$ ). Replacement of  $\text{HCO}_3^-$  with thiocyanate ( $\text{SCN}^-$ ) slightly shifted the reversal potential in a positive direction, but the inward conductance had little change (Fig. 2d;  $n = 6$ ). Finally, replacement of  $\text{HCO}_3^-$  with iodide ( $\text{I}^-$ ) did not

cause a marked difference in the reversal potential or the inward conductance (data not shown;  $n = 6$ ). We calculated the permeability ratio ( $P_X/P_{\text{HCO}_3}$ ) from the shift in the reversal potential ( $\Delta V_{\text{rev}}$ ) when anion X is substituted for internal  $\text{HCO}_3^-$  [13]; that is, from:

$$\Delta V_{\text{rev}} = (RT/F) \times \ln(P_X[X^-]_i/P_{\text{HCO}_3}[\text{HCO}_3^-]_i),$$

where R, T, and F have their conventional thermodynamic meanings. The sequence of the permeability ratios was:  $\text{SCN}^- (1.41 \pm 0.15) > \text{Cl}^- (1.18 \pm 0.14) = \text{glc}^- (1.07 \pm 0.03) = \text{I}^- (1.06 \pm 0.06) = \text{HCO}_3^- (1.00) > \text{MES}^- (0.65 \pm 0.11)$  ( $n = 5-6$ ). The sequence of the relative inward conductance determined from  $-80$  to  $-60$  mV was:  $\text{HCO}_3^- (1.00) > \text{SCN}^- (0.69 \pm 0.10) = \text{I}^- (0.66 \pm 0.09) > \text{Cl}^- (0.48 \pm 0.08) = \text{glc}^- (0.43 \pm 0.09) > \text{MES}^- (0.26 \pm 0.06)$  ( $n = 5-6$ ).

#### *Bicarbonate conductance is dependent on luminal $\text{Cl}^-$*

To evaluate the activities of  $\text{Cl}^-$ - $\text{HCO}_3^-$  exchangers on the apical membrane of interlobular pancreatic ducts of the guinea pig, Ishiguro and colleagues replaced  $\text{Cl}^-$  with gluconate in the lumen [14, 16, 44]. Similarly, we recorded macroscopic currents with extracellular solution containing 120 mM gluconate and 10 mM  $\text{Cl}^-$ . With the control intracellular solution,  $E_{\text{rev}}$  was  $-46.6 \pm 4.5$  mV with a standard NMDG-Cl pipette solution (Fig. 2a;  $n = 5$ ) and  $-63.6 \pm 3.9$  mV with gluconate-rich pipette solution (Fig. 3a;  $n = 5$ ), demonstrating a significant difference (ANOVA). We also compared the inward  $\text{HCO}_3^-$  conductance with gluconate-rich and standard NMDG-Cl pipette solutions (Fig. 3b). The  $\text{HCO}_3^-$  conductance was significantly lower with the gluconate-rich pipette solution ( $0.66 \pm 0.20$  nS) than with standard NMDG-Cl pipette solutions ( $1.30 \pm 0.09$  nS) ( $n = 5$ , ANOVA). Additionally, as described in the previous section, the inward conductance

significantly decreased when  $\text{HCO}_3^-$  in the bath was replaced with  $\text{Cl}^-$ , indicating that there was a minor contribution from  $\text{Cl}^-$ -dependent current (Fig. 3b, right). However, the inward conductance was not significantly different with gluconate-rich pipette solution (Fig. 3b, left). The results described so far indicate that both intracellular  $\text{HCO}_3^-$  and luminal  $\text{Cl}^-$  are essential for the  $\text{HCO}_3^-$  conductance, and that the  $\text{HCO}_3^-$  conductance is carried out through  $\text{Cl}^-$ - $\text{HCO}_3^-$  exchangers on the luminal membrane.

#### *Effects of the anion exchanger inhibitor H<sub>2</sub>DIDS on bicarbonate conductance*

Previous studies reported that  $\text{Cl}^-$ - $\text{HCO}_3^-$  exchangers were inhibited by luminal H<sub>2</sub>DIDS, a disulfonic stilbene [16, 44]. For experimental ease, we applied H<sub>2</sub>DIDS (0.5 mM) intracellularly while recording macroscopic currents from excised inside-out patches with the control bicarbonate internal and the standard NMDG-Cl pipette solutions. To exclude the possibility of the contamination of CFTR  $\text{Cl}^-$  conductance, we included 20  $\mu\text{M}$  CFTRinh-172, an inhibitor of CFTR  $\text{Cl}^-$  channels, in the pipette solution. H<sub>2</sub>DIDS applied intracellularly significantly decreased inward  $\text{HCO}_3^-$  conductance from  $1.57 \pm 0.55$  nS to  $0.86 \pm 0.37$  nS (Fig. 4;  $n = 6$ ). We also tested 30  $\mu\text{M}$  Sch28080, a  $\text{H}^+$ - $\text{K}^+$ -pump inhibitor, but did not observe any inhibitory effects on the inward  $\text{HCO}_3^-$  conductance ( $n = 4$ ; not shown). These results further support that the  $\text{HCO}_3^-$  conductance occurs through  $\text{Cl}^-$ - $\text{HCO}_3^-$  exchangers.

#### *Regulation of bicarbonate conductance by intracellular ATP and cAMP*

In pancreatic duct cells, cAMP and  $\text{Ca}^{2+}$  signaling pathways play a role in fluid secretion. As CFTR  $\text{Cl}^-$  channels were regulated by intracellular cAMP [6, 7, 30] and ATP [40], we tested their effects on bicarbonate conductance. Application of intracellular 2 mM ATP-

Mg significantly increased the inward conductance from  $1.51 \pm 0.59$  to  $5.70 \pm 2.18$  nS (Fig. 5a, b;  $n = 13$ ). The addition of 1 mM cAMP further increased the inward conductance to  $14.8 \pm 5.57$  nS ( $n = 4$ ). cAMP also activated the marked outward conductance, which was attributed to  $\text{Cl}^-$  influx, most likely through CFTR  $\text{Cl}^-$  channels. Therefore, we tested the effects of intracellular ATP-Mg and cAMP with the pipette solution including CFTRinh-172 at 20  $\mu\text{M}$ . In the presence of CFTRinh-172, application of intracellular 2 mM ATP-Mg and 1 mM cAMP had little effect on the conductance in either direction (Fig. 5c): the inward conductance was not significantly increased in the presence of ATP-Mg ( $1.11 \pm 0.39$  nS) or cAMP ( $1.37 \pm 0.27$  nS) as compared with the control ( $0.98 \pm 0.29$  nS) (Fig. 5d;  $n = 11$ ). These results indicate that intracellular ATP and cAMP may not directly regulate  $\text{Cl}^-$ - $\text{HCO}_3^-$  exchangers, but instead regulate CFTR  $\text{Cl}^-$  channels on the luminal membrane of duct cells. Additionally, 1  $\mu\text{M}$  free  $\text{Ca}^{2+}$  added to the intracellular solution did not affect the inward  $\text{HCO}_3^-$  conductance ( $n = 3$ ; not shown), suggesting that intracellular  $\text{Ca}^{2+}$  does not regulate  $\text{Cl}^-$ - $\text{HCO}_3^-$  exchangers directly.

#### *Pancreatic duct epithelia expressed a variety of SLC26A family members*

It is known that anion exchangers in pancreatic duct cells are members of the SLC26A family [26]. Two members of the family, SLC26A3 (DRA; down regulated in adenoma) [25] and SLC26A6 (PAT1; putative anion transporter-1) [24, 46], were reported to be expressed in the luminal membrane of pancreatic ducts and function as  $\text{Cl}^-$ - $\text{HCO}_3^-$  exchangers [9, 19, 20]. Interlobular ducts from guinea pigs expressed mRNAs encoding *Slc26a3* and *Slc26a6* [44]. In the present study, we evaluated the expression of all members of the SLC26A family using RT-PCR analysis on isolated

interlobular and main ducts. Figure 6a shows the isolated interlobular and main pancreatic ducts expressing CFTR and GAPDH. Then, we screened all eleven members of the SLC26A family from the interlobular ducts (Fig. 6b;  $n = 3$  animals) and main ducts (Fig. 6c;  $n = 3$  animals), along with GAPDH and a duct marker of carbonic anhydrase II (CA2). We also screened all primer sets from the total RNA of the kidney as a positive control (Fig. 6d). RT-PCR analysis revealed that the interlobular and main ducts expressed *Slc26a1*, *Slc26a2*, *Slc26a3*, *Slc26a4*, *Slc26a6*, *Slc26a7*, *Slc26a9*, *Slc26a10*, and *Slc26a11*.

#### *Immunolocalization of the SLC26A family in pancreatic duct cells*

The immunolocalization of the SLC26A family was examined with paraffin sections of guinea pig pancreas. Immunofluorescence ascribed to the SLC26A exchanger was colocalized with Ezrin, an A-kinase anchoring protein, to the luminal membrane of the pancreatic duct (Fig. 7). In the guinea pig pancreas, immunofluorescence of SLC26A6 was detected on the luminal membranes of duct cells (Fig. 7a), as reported for the rat pancreas previously [20]. SLC26A6 were colocalized with Ezrin to the luminal membranes (Fig. 7b, c). The immunofluorescence on the luminal membranes was diminished with SLC26A6 antibody, which was pre-absorbed with the corresponding antigen for the negative control (Fig. 7d). Additionally, a strong signal ascribed to SLC26A1 was detected and colocalized with Ezrin to the luminal membrane (Fig. 7e–g). We also detected immunofluorescence of SLC26A4 and SLC26A10 on the luminal membrane of the duct cells (Fig. 7i–k and m–o, respectively). The immunofluorescence was reduced when antibodies were pre-absorbed with the corresponding antigens (Fig. 7h, l, p). We used HPA036055 (Atlas) as the anti-SLC26A3 antibody, but failed to

immunostain SLC26A3 in the guinea pig pancreas. We stained with PECAM-1, a blood vessel marker, to distinguish between pancreatic ducts and blood vessels (Fig. 7q, r).

#### *Expression of SLC26A protein in guinea pig pancreatic ducts*

We next performed western blot analysis to examine the expression of SLC26A protein in the guinea pig pancreatic ducts. We detected SLC26A6 (~107 kDa), SLC26A1 (~78 kDa), SLC26A4 (~136 kDa), and SLC26A10 (~108 kDa) in the lysates of the isolated ducts (Fig. 8;  $n = 3$  animals). The molecular mass values corresponded to those of human SLC26A proteins (~100 kDa), which were *N*-glycosylated, expressed in HEK-293 cells [22].

## **Discussion**

In the present study, we applied patch electrodes on the luminal membrane of guinea pig pancreatic duct cells and recorded macroscopic currents in the inside-out configuration. The inward conductance was dependent on the intracellular  $\text{HCO}_3^-$  concentration (Fig. 1) and was reduced when intracellular  $\text{HCO}_3^-$  was replaced with  $\text{Cl}^-$ ,  $\text{glc}^-$ , or  $\text{MES}^-$  (Fig. 2) or extracellular  $\text{Cl}^-$  was replaced with  $\text{glc}^-$  (Fig. 3). Furthermore, the inward conductance was decreased in the presence of  $\text{H}_2\text{DIDS}$ , an inhibitor of  $\text{Cl}^-$ - $\text{HCO}_3^-$  exchangers (Fig. 4). These electrophysiological findings suggested that the inward conductance was ascribed to  $\text{HCO}_3^-$  efflux through  $\text{Cl}^-$ - $\text{HCO}_3^-$  exchangers on the luminal membrane. In addition, we found that SLC26A1, SLC26A4, SLC26A6, and SLC26A10 were localized to the luminal membrane of the pancreatic duct cells (Figs. 7

and 8).

$\text{HCO}_3^-$  can flow outwardly not only through  $\text{Cl}^-$ - $\text{HCO}_3^-$  exchangers but also through CFTR  $\text{Cl}^-$  channels on the luminal membrane [8]. The permeability ratio sequence of the  $\text{Cl}^-$  channel in inside-out patches from the rat pancreatic duct cells was:  $\text{NO}_3^- > \text{Cl}^- > \text{HCO}_3^- > \text{gluconate}$  [8], and that in whole-cell patches from the guinea pig pancreatic duct cells was:  $\text{Br}^- > \Gamma^- = \text{Cl}^- > \text{HCO}_3^- > \text{ClO}_4^- > \text{aspartate}$  [30]. These were different from the permeability ratio sequence of the inward conductance obtained in the present study:  $\text{SCN}^- > \text{Cl}^- = \text{gluconate} = \Gamma^- = \text{HCO}_3^- > \text{MES}^-$  (Fig. 2). Similarly, a previous study reported that the anion selectivity of SLC26A6 in HEK 293 cells was  $\text{SCN}^- > \text{NO}_3^- > \text{Cl}^-$  [29]. Single-channel and whole-cell conductance through  $\text{Cl}^-$  channels was reduced in the presence of  $\text{HCO}_3^-$  [8, 30], whereas the inward conductance was increased with increasing intracellular  $\text{HCO}_3^-$  in our experiments (Fig. 1). These results suggest that  $\text{HCO}_3^-$  efflux occurs by pathway independent from the  $\text{Cl}^-$  channels. We followed previous studies that evaluated the activities of  $\text{Cl}^-$ - $\text{HCO}_3^-$  exchangers on the apical membrane of pancreatic ducts by replacing extracellular  $\text{Cl}^-$  with gluconate [14, 16, 44], and observed that the reversal potential shifted to a negative direction and the inward  $\text{HCO}_3^-$  conductance decreased (Fig. 3). The dependency of inward  $\text{HCO}_3^-$  conductance on extracellular  $\text{Cl}^-$  suggests that  $\text{HCO}_3^-$  is exchanged for  $\text{Cl}^-$ . Our results demonstrated that intracellular  $\text{HCO}_3^-$  increased the conductance with a  $K_d$  value of approximately 30 mM (Fig. 1), corresponding to the physiological concentration of intracellular  $\text{HCO}_3^-$  in duct cells. Additionally, the Hill coefficient, which was estimated to be 3.5 for the effects of  $\text{HCO}_3^-$ , suggested that positive cooperative binding of  $\text{HCO}_3^-$  facilitated the binding of subsequent  $\text{HCO}_3^-$  at other sites on  $\text{Cl}^-$ - $\text{HCO}_3^-$  exchangers.

We detected SLC26A1, SLC26A4, SLC26A6, and SLC26A10 on the luminal membrane of the interlobular pancreatic duct (Fig. 7). SLC26A6 was localized to the luminal membrane of interlobular pancreatic ducts of humans [24] and rats [20], as well as to the intestine, kidney, parotid gland, and heart [1, 20, 21, 24, 48]. SLC26A6 cloned from guinea pig pancreatic ducts mediated  $\text{Cl}^-$ - $\text{HCO}_3^-$  exchange in HEK 293 cells [43]. SLC26A4 (pendrin) was localized to the apical membranes of the submandibular duct, type B and non-A, non-B intercalated cells in the cortical collecting duct of the kidney, and thyroid follicular cells, and was expressed in inner ear [3, 36, 37, 39]. SLC26A4 mediates  $\text{HCO}_3^-$  secretion across the apical membrane in Calu-3, a human airway epithelia cell line, monolayers [5] and in the cortical collecting ducts [37]. SLC26A1 identified as sulfate/bicarbonate/oxalate exchangers was expressed in the liver and kidney, and to a lesser extent, in the pancreas and testis [2, 35], and detected on the basolateral membrane of kidney and liver epithelial cells [18, 34]. SLC26A10 was found at the mRNA level in the heart and sarcoma [1, 4], but its function is unknown. Although the previous study demonstrated localization of SLC26A3 to the apical membrane of mouse pancreatic duct cells [9], we were unable to immunostain SLC26A3 in guinea pig pancreatic duct cells. The immunostaining signal in the guinea pig pancreas may be underestimated because we were only able to use antibodies against the human SLC26A family. Future studies are needed to establish the functional relevance of SLC26A molecules in pancreatic ducts.

We found that intracellular ATP and cAMP activated anion conductance on the luminal membrane in guinea pig pancreatic duct cells (Fig. 5a, b), as observed in rat pancreatic

duct cells [6]. It was reported using HEK293 cells that CFTR stimulated by forskolin activated anion exchange of SLC26A3, SLC26A4, and SLC26A6 [19]. Thus, the increased conductance was attributed to activation of CFTR  $\text{Cl}^-$  channels by intracellular ATP and cAMP [6, 7, 30, 40], and activation of  $\text{Cl}^-$ - $\text{HCO}_3^-$  exchangers by activated CFTR [19]. As anion conductance was not significantly increased in the presence of CFTRinh-172 in the pipette solution (Fig. 5c, d), we concluded that intracellular ATP and cAMP may not directly regulate  $\text{Cl}^-$ - $\text{HCO}_3^-$  exchangers.

We found that H<sub>2</sub>DIDS applied intracellularly inhibited inward  $\text{HCO}_3^-$  conductance by 50% in excised inside-out patches from the luminal membrane (Fig. 4). A previous study demonstrated that other disulfonic stilbenes, 4,4'-dinitrostilbene-2,2'-disulphonic acid and 4,4'-diisothiocyanostilbene-2,2'-disulfonic acid, blocked CFTR  $\text{Cl}^-$  channels when applied to the cytoplasmic face of membrane patches, with  $K_d$  values (at 0 mV) of 160  $\mu\text{M}$  and 80  $\mu\text{M}$ , respectively [23]. It is likely that disulfonic stilbenes are able to act on  $\text{Cl}^-$ - $\text{HCO}_3^-$  exchangers from not only the outside but also from the inside of the cell membrane.

In conclusion, we used the patch clamp technique in the inside-out configuration and demonstrated that the  $\text{HCO}_3^-$  conductance through the luminal membrane is mediated by  $\text{Cl}^-$ - $\text{HCO}_3^-$  exchangers under physiological  $\text{HCO}_3^-$  concentrations in pancreatic duct cells. Our findings suggest that SLC26A1, SLC26A4, SLC26A6, and SLC26A10 may be involved in the  $\text{HCO}_3^-$  transport through the luminal membrane. The SLC26A family may also play a role in pH homeostasis in the pancreatic lumen and duct cells. The direct measurement of the  $\text{HCO}_3^-$  current from the interlobular duct and its functional

characterization helps to propose a useful model for  $\text{HCO}_3^-$  secretion from the pancreatic duct epithelia (Fig. 9).

## Reference list

1. **Alvarez BV, Kieller DM, Quon AL, Markovich D, Casey JR** (2004) Slc26a6: a cardiac chloride–hydroxyl exchanger and predominant chloride–bicarbonate exchanger of the mouse heart. *J. Physiol* 561:721–734. doi:10.1113/jphysiol.2004.077339
2. **Bissig M, Hagenbuch B, Stieger B, Koller T, Meier PJ** (1994) Functional expression cloning of the canalicular sulfate transport system of rat hepatocytes. *J Biol Chem* 269:3017–3021. PMID: 8300633
3. **Everett LA, Morsli H, Wu DK, Green ED** (1999) Expression pattern of the mouse ortholog of the pendred’s syndrome gene (*Pds*) suggests a key role for pendrin in the inner ear. *Proc Natl Acad Sci USA* 96:9727–9732. doi: 10.1073/pnas.96.17.9727
4. **Francis P, Namløs HM, Müller C, Edén P, Fernebro J, Berner JM, Bjerkehagen B, Åkerman M, Bendahl PO, Isinger A, Rydholm A, Myklebost O, Nilbert M** (2007) Diagnostic and prognostic gene expression signatures in 177 soft tissue sarcomas: hypoxia-induced transcription profile signifies metastatic potential. *BMC Genomics* 8:73. doi: 10.1186/1471-2164-8-73
5. **Garnett JP, Hickman E, Burrows R, Hegyi P, Tizslavicz L, Cuthbert AW, Fong P, Gray MA** (2011) Novel role for pendrin in orchestrating bicarbonate secretion in cystic fibrosis transmembrane conductance regulator (CFTR)-expressing airway serous cells. *J Biol Chem* 286:41069–41082. doi: 10.1074/jbc.M111.266734
6. **Gray MA, Greenwell JR, Argent BE** (1988) Secretin-regulated chloride channel on the apical plasma membrane of pancreatic duct cells. *J Membr Biol* 105:131–142. doi: 10.1007/BF02009166
7. **Gray MA, Plant S, Argent BE** (1993) cAMP-regulated whole cell chloride currents in pancreatic duct cells. *Am J Physiol* 264:C591–C602. PMID: 7681623

8. **Gray MA, Pollard CE, Harris A, Coleman L, Greenwell JR, Argent BE** (1990) Anion selectivity and block of the small-conductance chloride channel on pancreatic duct cells. *Am J Physiol* 259:C752–C761. PMID: 1700622
9. **Greeley T, Shumaker H, Wang Z, Schweinfest CW, Soleimani M** (2001) Downregulated in adenoma and putative anion transporter are regulated by CFTR in cultured pancreatic duct cells. *Am J Physiol Gastrointest Liver Physiol* 281:G1301–G1308. PMID: 11668039
10. **Hayashi M, Inagaki A, Novak I, Matsuda H** (2016) The adenosine A<sub>2B</sub> receptor is involved in anion secretion in human pancreatic duct Capan-1 epithelial cells. *Pflügers Arch* 468:1171–1181. doi: 10.1007/s00424-016-1806-9
11. **Hayashi M, Novak I** (2013) Molecular basis of potassium channels in pancreatic duct epithelial cells. *Channels (Austin)* 7:432–441. doi: 10.4161/chan.26100
12. **Hayashi M, Wang J, Hede SE, Nova I** (2012) An intermediate-conductance Ca<sup>2+</sup>-activated K<sup>+</sup> channel is important for secretion in pancreatic duct cells. *Am J Physiol Cell Physiol* 303:C151–C159. doi: 10.1152/ajpcell.00089.2012
13. **Hille B** (2001) *Ionic Channels of Excitable Membranes*, 3rd edn. Sinauer Associates, Sunderland
14. **Ishiguro H, Namkung W, Yamamoto A, Wang Z, Worrell RT, Xu J, Lee MG, Soleimani M** (2007) Effect of Slc26a6 deletion on apical Cl<sup>-</sup>/HCO<sub>3</sub><sup>-</sup> exchanger activity and cAMP-stimulated bicarbonate secretion in pancreatic duct. *Am J Physiol Gastrointest Liver Physiol* 292:G447–G455. doi: 10.1152/ajpgi.00286.2006
15. **Ishiguro H, Naruse S, Kitagawa M, Mabuchi T, Kondo T, Hayakawa T, Case RM, Steward MC** (2002) Chloride transport in microperfused interlobular ducts isolated from guinea-pig pancreas. *J Physiol* 539:175–189. doi: 10.1113/jphysiol.2001.012490
16. **Ishiguro H, Naruse S, Steward MC, Kitagawa M, Ko SB, Hayakawa T, Case RM** (1998) Fluid secretion in interlobular ducts isolated from guinea-pig pancreas. *J Physiol* 511:407–422. doi: 10.1111/j.1469-7793.1998.407bh.x
17. **Ishiguro H, Steward MC, Naruse S, Ko SB, Goto H, Case RM, Kondo T, Yamamoto A** (2009) CFTR functions as a bicarbonate channel in pancreatic duct cells. *J Gen Physiol* 133:315–326. doi: 10.1085/jgp.200810122
18. **Karniski LP, Lötscher M, Fucntese M, Hilfiker H, Biber J, Murer H** (1998) Immunolocalization of sat-1 sulfate/oxalate/bicarbonate anion exchanger in the rat kidney. *Am J Physiol* 275:F79–F87. PMID: 9689008

19. **Ko SB, Shcheynikov N, Choi JY, Luo X, Ishibashi K, Thomas PJ, Kim JY, Kim KH, Lee MG, Naruse S, Muallem S** (2002) A molecular mechanism for aberrant CFTR-dependent  $\text{HCO}_3^-$  transport in cystic fibrosis. *EMBO J* 21:5662–5672. doi: 10.1093/emboj/cdf580
20. **Ko SB, Zeng W, Dorwart MR, Luo X, Kim KH, Millen L, Goto H, Naruse S, Soyombo A, Thomas PJ, Muallem S** (2004) Gating of CFTR by the STAS domain of SLC26 transporters. *Nat Cell Biol* 6:343–350. doi:10.1038/ncb1115
21. **Kujala M, Tienari J, Lohi H, Elomaa O, Sariola H, Lehtonen E, Kere J** (2005) SLC26A6 and SLC26A7 anion exchangers have a distinct distribution in human kidney. *Nephron Exp Nephrol* 101:e50–e58. doi: 10.1159/000086345
22. **Li J, Xia F, Reithmeier RA** (2014) *N*-glycosylation and topology of the human SLC26 family of anion transport membrane proteins. *Am J Physiol Cell Physiol* 306:C943–C960. doi: 10.1152/ajpcell.00030.2014
23. **Linsdell P, Hanrahan JW** (1996) Disulphonic stilbene block of cystic fibrosis transmembrane conductance regulator  $\text{Cl}^-$  channels expressed in a mammalian cell line and its regulation by a critical pore residue. *J Physiol* 496:687–693. doi: 10.1113/jphysiol.1996.sp021719
24. **Lohi H, Kujala M, Kerkelä E, Saarialho-Kere U, Kestilä M, Kere J** (2000) Mapping of five new putative anion transporter genes in human and characterization of SLC26A6, a candidate gene for pancreatic anion exchanger. *Genomics* 70:102–112. doi: 10.1006/geno.2000.6355
25. **Melvin JE, Park K, Richardson L, Schultheis PJ, Shull GE** (1999) Mouse down-regulated in adenoma (DRA) is an intestinal  $\text{Cl}^-/\text{HCO}_3^-$  exchanger and is up-regulated in colon of mice lacking the NHE3  $\text{Na}^+/\text{H}^+$  exchanger. *J Biol Chem* 274:22855–22861. doi:10.1074/jbc.274.32.22855
26. **Mount DB, Romero MF** (2004) The SLC26 gene family of multifunctional anion exchangers. *Pflügers Arch* 447:710–721. doi: 10.1007/s00424-003-1090-3
27. **Novak I, Greger R** (1988) Properties of the luminal membrane of isolated perfused rat pancreatic ducts. Effect of cyclic AMP and blockers of chloride transport. *Pflügers Arch* 411:546–553. PMID: 2455270
28. **Novak I, Wang J, Henriksen KL, Haanes KA, Krabbe S, Nitschke R, Hede SE** (2011) Pancreatic bicarbonate secretion involves two proton pumps. *J Biol Chem* 286:280–289. doi: 10.1074/jbc.M110.136382
29. **Ohana E, Shcheynikov N, Yang D, So I, Muallem S** (2011) Determinants of coupled transport and uncoupled current by the electrogenic SLC26

- transporters. *J Gen Physiol* 137:239–251. doi: 10.1085/jgp.201010531
30. **O'Reilly CM, Winpenny JP, Argent BE, Gray MA** (2000) Cystic fibrosis transmembrane conductance regulator currents in guinea pig pancreatic duct cells: inhibition by bicarbonate ions. *Gastroenterology* 118:1187–1196. doi: 10.1016/S0016-5085(00)70372-6
  31. **Park HW, Nam JH, Kim JY, Namkung W, Yoon JS, Lee JS, Kim KS, Venglovecz V, Gray MA, Kim KH, Lee MG** (2010) Dynamic regulation of CFTR bicarbonate permeability by  $[Cl^-]_i$  and its role in pancreatic bicarbonate secretion. *Gastroenterology* 139:620–631. doi: 10.1053/j.gastro.2010.04.004
  32. **Petersen OH, Courjaret R, Machaca K** (2017)  $Ca^{2+}$  tunnelling through the ER lumen as a mechanism for delivering  $Ca^{2+}$  entering via store-operated  $Ca^{2+}$  channels to specific target sites. *J Physiol* 595:2999–3014. doi: 10.1113/JP272772
  33. **Petersen OH, Ueda N** (1977) Secretion of fluid and amylase in the perfused rat pancreas. *J Physiol* 264:819–835. PMID: 191595
  34. **Quondamatteo F, Krick W, Hagos Y, Kruger MH, Neubauer-saile K, Herken R, Ramadori G, Burckhardt G, Burckhardt BC** (2006) Localization of the sulfate/anion exchanger in the rat liver. *Am J Physiol Gastrointest Liver Physiol* 290:G1075–G1081. doi:10.1152/ajpgi.00492.2005
  35. **Regeer RR, Lee A, Markovich D** (2003) Characterization of the human sulfate anion transporter (hsat-1) protein and gene (SAT1; SLC26A1). *DNA Cell Biol* 22:107–117. doi: 10.1089/104454903321515913
  36. **Royaux IE, Suzuki K, Mori A, Katoh R, Everett LA, Kohn LD, Green ED** (2000) Pendrin, the protein encoded by the pendred syndrome gene (*PDS*), is an apical porter of iodide in the thyroid and is regulated by thyroglobulin in FRTL-5 cells. *Endocrinology* 141:839–845. doi: 10.1210/endo.141.2.7303
  37. **Royaux IE, Wall SM, Karniski LP, Everett LA, Suzuki K, Knepper MA, Green ED** (2001) Pendrin, encoded by the pendred syndrome gene, resides in the apical region of renal intercalated cells and mediates bicarbonate secretion. *Proc Natl Acad Sci USA* 98:4221–4226. doi: 10.1073/pnas.071516798
  38. **Shcheynikov N, Wang Y, Park M, Ko SB, Dorwart M, Naruse S, Thomas PJ, Muallem S** (2006) Coupling modes and stoichiometry of  $Cl^-/HCO_3^-$  exchange by *slc26a3* and *slc26a6*. *J Gen Physiol* 127:511–524. doi:10.1085/jgp.200509392
  39. **Shcheynikov N, Yang D, Wang Y, Zeng W, Karniski LP, So I, Wall SM, Muallem S** (2008) The *Slc26a4* transporter functions as an electroneutral

- Cl<sup>-</sup>/Γ/HCO<sub>3</sub><sup>-</sup> exchanger: role of Slc26a4 and Slc26a6 in Γ<sup>-</sup> and HCO<sub>3</sub><sup>-</sup> secretion and in regulation of CFTR in the parotid duct. *J Physiol* 586:3813–3824. doi: 10.1113/jphysiol.2008.154468
40. **Sheppard DN, Welsh MJ** (1999) Structure and function of the CFTR chloride channel. *Physiol Rev* 79:S23–S45. PMID: 9922375
  41. **Song Y, Yamamoto A, Steward MC, Ko SB, Stewart AK, Soleimani M, Liu BC, Kondo T, Jin CX, Ishiguro H** (2012) Deletion of Slc26a6 alters the stoichiometry of apical Cl<sup>-</sup>/HCO<sub>3</sub><sup>-</sup> exchange in mouse pancreatic duct. *Am J Physiol Cell Physiol* 303:C815–C824. doi: 10.1152/ajpcell.00151.2012
  42. **Steward MC, Ishiguro H, Case RM** (2005) Mechanisms of bicarbonate secretion in the pancreatic duct. *Annu Rev Physiol* 67:377–409. doi: 10.1146/annurev.physiol.67.031103.153247
  43. **Stewart AK, Shmukler BE, Vandorpe DH, Reimold F, Heneghan JF, Nakakuki M, Akhavein A, Ko S, Ishiguro H, Alper SL** (2011) SLC26 anion exchangers of guinea pig pancreatic duct: molecular cloning and functional characterization. *Am J Physiol Cell Physiol* 301:C289–C303. doi: 10.1152/ajpcell.00089.2011
  44. **Stewart AK, Yamamoto A, Nakakuki M, Kondo T, Alper SL, Ishiguro H** (2009) Functional coupling of apical Cl<sup>-</sup>/HCO<sub>3</sub><sup>-</sup> exchange with CFTR in stimulated HCO<sub>3</sub><sup>-</sup> secretion by guinea pig interlobular pancreatic duct. *Am J Physiol Gastrointest Liver Physiol* 296:G1307–G1317. doi:10.1152/ajpgi.90697.2008
  45. **Venglovecz V, Hegyi P, Rakonczay Z Jr, Tiszlavicz L, Nardi A, Grunnet M, Gray MA** (2011) Pathophysiological relevance of apical large conductance Ca<sup>2+</sup>-activated potassium channels in pancreatic duct epithelial cells. *Gut* 60:361–369. doi: 10.1136/gut.2010.214213
  46. **Waldegger S, Moschen I, Ramirez A, Smith RJ, Ayadi H, Lang F, Kubisch C** (2001) Cloning and characterization of *SLC26A6*, a novel member of the solute carrier 26 gene family. *Genomics* 72:43–50. doi: 10.1006/geno.2000.6445
  47. **Wang Y, Soyombo AA, Shcheynikov N, Zeng W, Dorwart M, Marino CR, Thomas PJ, Muallem S** (2006) Slc26a6 regulates CFTR activity *in vivo* to determine pancreatic duct HCO<sub>3</sub><sup>-</sup> secretion: relevance to cystic fibrosis. *EMBO J* 25:5049–5057. doi: 10.1038/sj.emboj.7601387
  48. **Wang Z, Petrovic S, Mann E, Soleimani M** (2002) Identification of an apical Cl<sup>-</sup>/HCO<sub>3</sub><sup>-</sup> exchanger in the small intestine. *Am J Physiol Gastrointest Liver*

- Physiol 282:G573–G579. doi: 10.1152/ajpgi.00338.2001
49. **Wilschanski M, Novak I** (2013) The cystic fibrosis of exocrine pancreas. *Cold Spring Harb Perspect Med* 3:a009746. doi: 10.1101/cshperspect.a009746
50. **Yamaguchi M, Steward MC, Smallbone K, Sohma Y, Yamamoto A, Ko SB, Kondo T, Ishiguro H** (2017) Bicarbonate-rich fluid secretion predicted by a computational model of guinea-pig pancreatic duct epithelium. *J Physiol* 595:1947–1972. doi: 10.1113/JP273306

Table 1. Primer sets used for guinea pig pancreatic duct in RT-PCR analysis

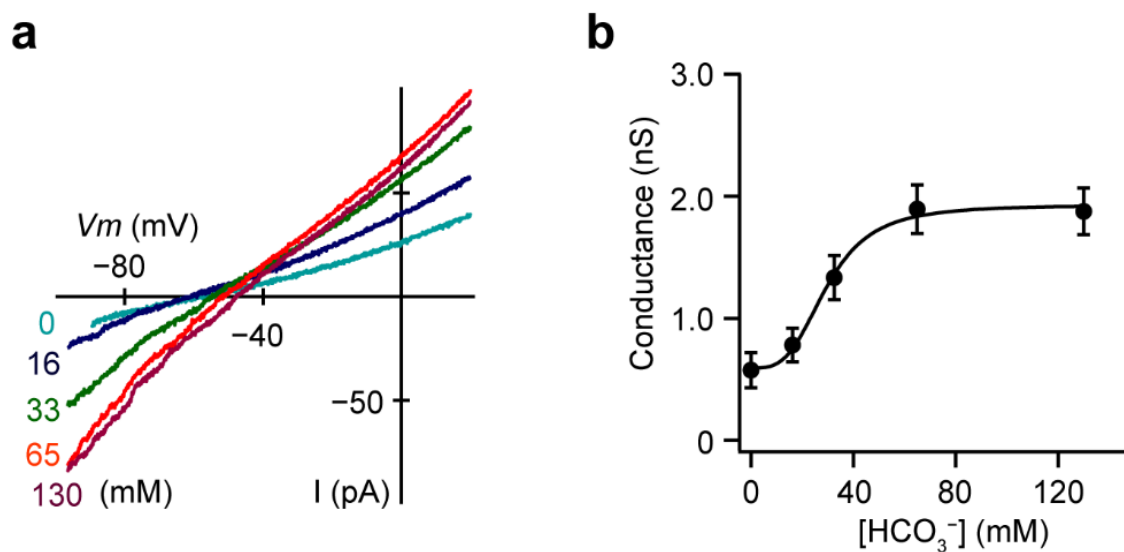
Gene (Subunit)		Size (bp)
Cftr		
Forward:	5'-GCTTAAAAGGACTATGGACACT -3'	623
Reverse:	5'-ACCTTCAGTG TTCAGCAGTCT -3'	
Gapdh		
Forward:	5'-CAAAGGGTCATCATCTCTGC -3'	610
Reverse:	5'-GCCGAACTCATTGTCATACCA -3'	
CA2		
Forward:	5'-AGCCTCTGCACCTTCACTATG -3'	535
Reverse:	5'-AACATCTGCTCACTGCTTACG -3'	
Slc26a1		
Forward:	5'-CTACTCTGTCCGTGCCAACCA -3'	914
Reverse:	5'-ACAGCTGCTCATCCTCCATTC -3'	
Slc26a2		
Forward:	5'-GGGGTTGGTTTTTCTATGTTTTG -3'	554
Reverse:	5'-AAACCCACCGCTTCATACACG -3'	
Slc26a3		
Forward:	5'-GTATGAGCCAGAAGGAGTGAA -3'	459
Reverse:	5'-TACACATCTACATTTATCCTTGC -3'	
Slc26a4		
Forward:	5'-AAACATCCCCACCACAGACAT -3'	558
Reverse:	5'-AAACCACATTGCTCCATCTGC -3'	
Slc26a5		
Forward:	5'-GTGACCTTGCTCTCGGGAAT -3'	621
Reverse:	5'-GAAGAGGGAGCCGATGGAAT-3'	
Slc26a6		
Forward:	5'-TCGGTCCTCAGCCACTTTGTA -3'	544
Reverse:	5'-ATGCTGCTTGGTGATAGATGC-3'	
Slc26a7		
Forward:	5'-CCCCAATGAACCTCCTGTCTG-3'	713
Reverse:	5'-AAGTAGGTGATTAGTGGCATTTC-3'	
Slc26a8		
Forward:	5'-TCGGGGCTTGGTCGTCTTG-3'	646
Reverse:	5'-AGGTTGATAGATGGGCTGGTA-3'	
Slc26a9		

Forward:	5'-CTATCTGTACCCTCTCCCTAA -3'	721
Reverse:	5'-AACGAGGGTATGGAAGGTAAC -3'	
Slc26a10		
Forward:	5'-ACTTTGCTGTGTGGATGGTCA-3'	550
Reverse:	5'-GCATCCTGGACACTCACAAAC-3'	
Slc26a11		
Forward:	5'-CAGGCAGCTTTGGGCGGAC-3'	566
Reverse:	5'-AGAGAAAACCAGGGAGACACC-3'	

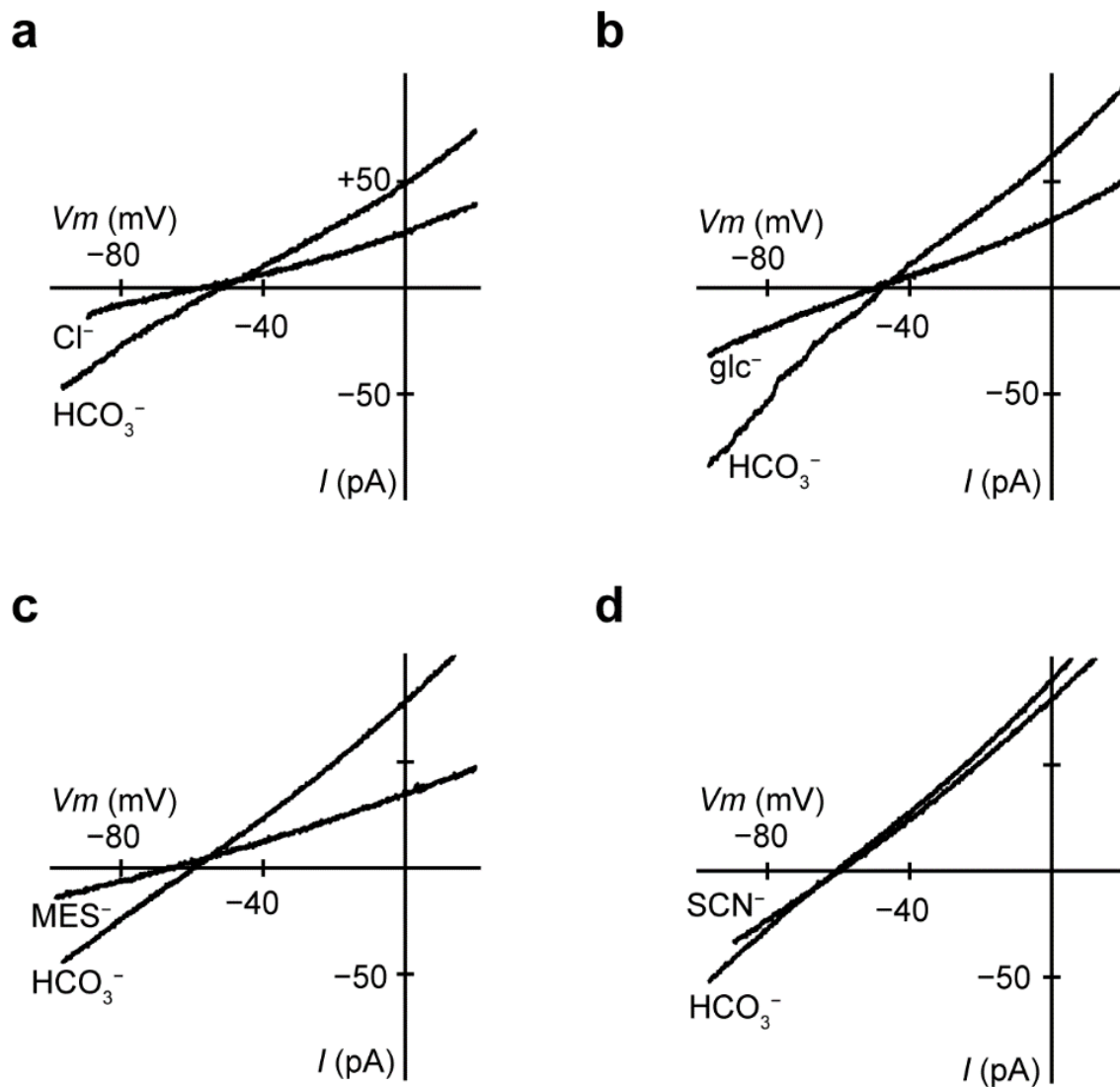
---

Table 2. Antibodies used for guinea pig pancreatic duct in immunohistochemistry (IHC) and western blotting (WB)

Protein (accession)	Antigen	Correlation with guinea pig	Dilution		Catalogue number (manufacturer)
			IHC	WB	
SLC26A1 (NP_071325)	518–587	77%	1:100	1:500	HPA041654 (Atlas)
SLC26A3 (NP_000102)	617–733	85%	1:100	N/A	HPA036055 (Atlas)
SLC26A4 (NP_000432)	317–344	93%	1:200	1:1000	bs-6787R (Bioss antibodies)
SLC26A6 (NP_075062)	438–484	83%	1:200	1:1000	bs-20817R (Bioss antibodies)
SLC26A10 (NP_597996)	427–487	75%	1:200	1:100	HPA044719 (Atlas)



**Fig. 1** Bicarbonate conductance through the luminal membrane of the interlobular pancreatic duct cells. **a** Macroscopic current–voltage ( $I$ – $V$ ) relationships recorded from the luminal membrane of the pancreatic duct cells in the inside-out configuration with the standard NMDG-Cl pipette solution at different intracellular  $\text{HCO}_3^-$  concentrations. Inward conductance attributed to  $\text{HCO}_3^-$  efflux increased with  $\text{HCO}_3^-$  concentration from 0 to 130 mM. **b** Linear plot of conductance by the  $\text{HCO}_3^-$  concentration. The solid line is the fit by the Hill equation with the half-maximal effective concentration of  $31.5 \pm 5.1$  mM and a Hill coefficient of  $3.5 \pm 0.4$  ( $n = 5$ )



**Fig. 2** Ion selectivity of bicarbonate conductance. Macroscopic  $I-V$  relationships recorded from different inside-out patches. The intracellular 130 mM  $\text{HCO}_3^-$  was substituted by equimolar chloride ( $\text{Cl}^-$ ), gluconate ( $\text{glc}^-$ ), methanesulfonate ( $\text{MES}^-$ ), or thiocyanate ( $\text{SCN}^-$ ) ( $n = 5-6$ ). The inward conductance decreased significantly when  $\text{HCO}_3^-$  was substituted with  $\text{Cl}^-$ ,  $\text{glc}^-$ , or  $\text{MES}^-$

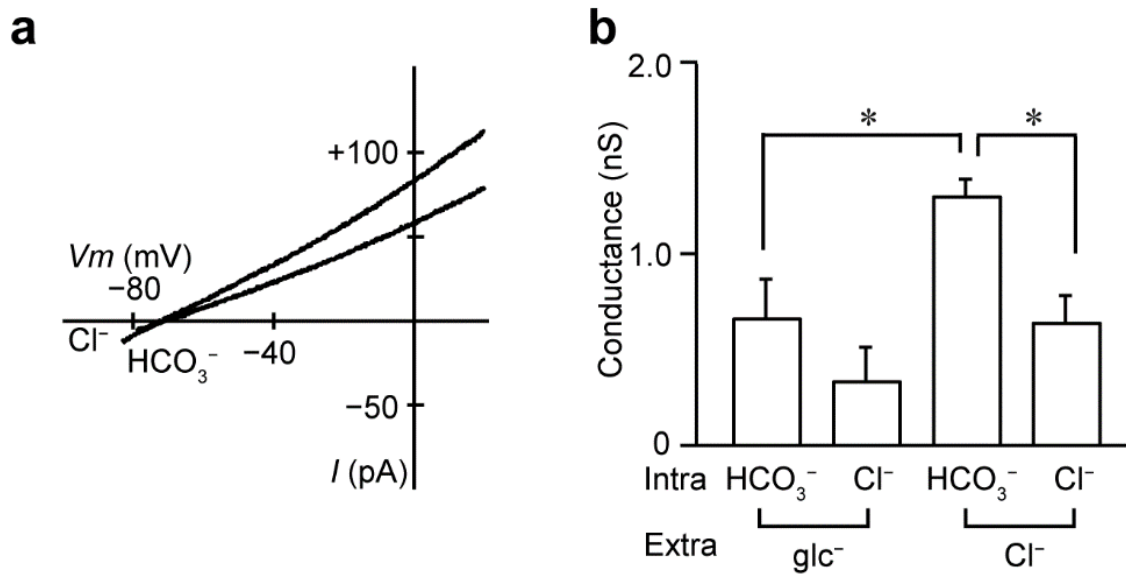


**Fig. 3** Effects of substitution of extracellular  $\text{Cl}^-$  with gluconate. **a** Macroscopic  $I-V$  relationships recorded from the interlobular pancreatic duct cells with gluconate-rich extracellular and 130 mM- $\text{HCO}_3^-$  or 130 mM- $\text{Cl}^-$  intracellular solutions. **b** The inward conductance attributed to efflux of  $\text{HCO}_3^-$  or  $\text{Cl}^-$  with gluconate-rich and standard NMDG-Cl pipette solutions ( $n = 5$ ,  $*P < 0.05$ , ANOVA). Intra and Extra, intracellular and extracellular, respectively

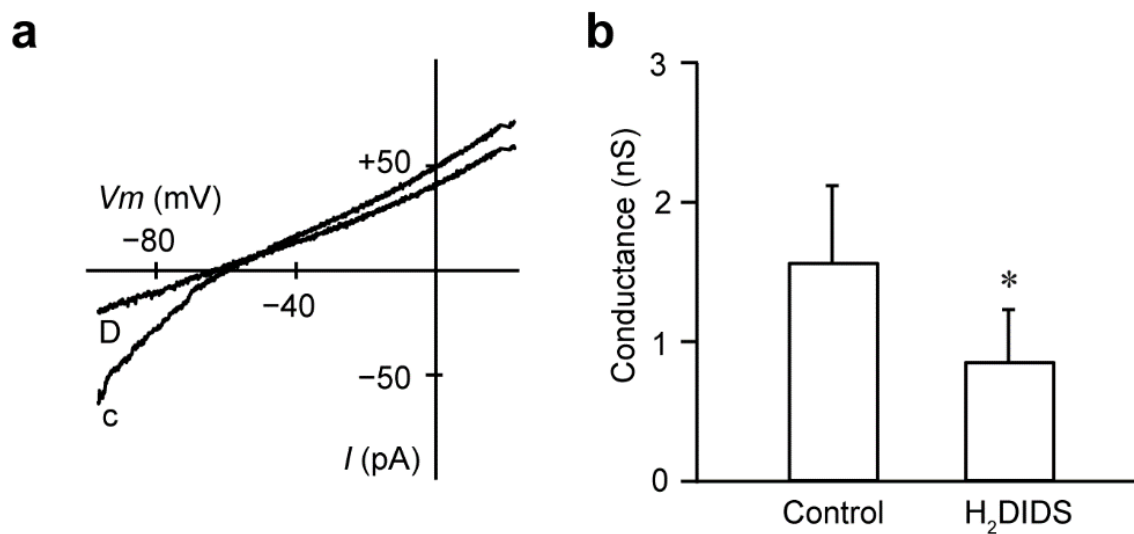


**Fig. 4** Effects of H<sub>2</sub>DIDS on bicarbonate conductance. **a** Macroscopic  $I$ - $V$  relationships obtained in the absence or presence of 0.5 mM intracellular H<sub>2</sub>DIDS. c, control; D, H<sub>2</sub>DIDS. CFTRinh-172 at 20  $\mu$ M was added to the standard NMDG-Cl pipette solution. **b** H<sub>2</sub>DIDS significantly decreased the average inward HCO<sub>3</sub><sup>-</sup> conductance ( $n = 6$ , \* $P < 0.05$ )

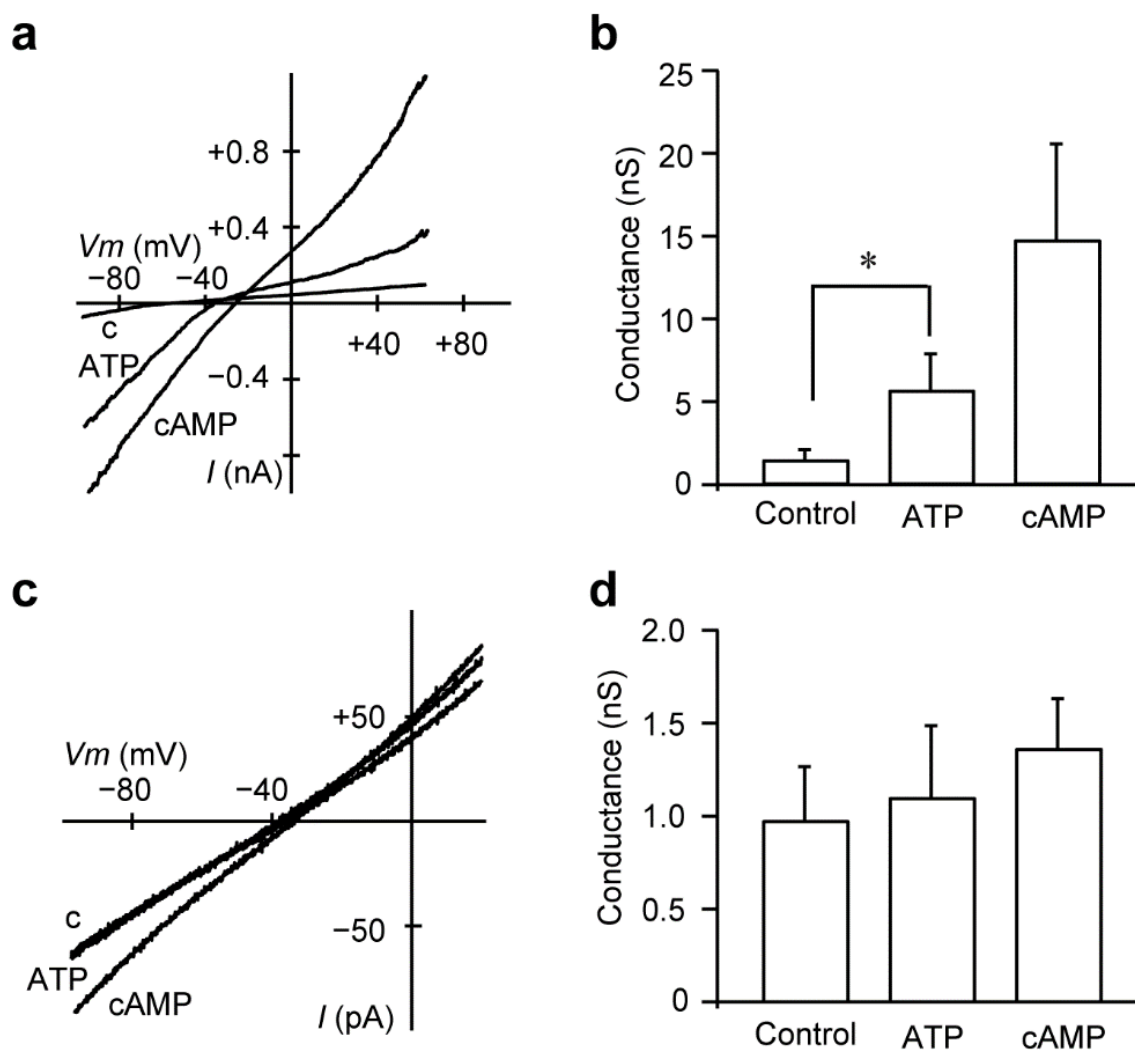


**Fig. 5** Activation of bicarbonate conductance by intracellular ATP and cAMP. **a** Macroscopic  $I$ - $V$  relationships from the interlobular pancreatic duct cells with the control bicarbonate internal solution (c), and with addition of ATP alone, or ATP and cAMP. The standard NMDG-Cl pipette solution was used. **b** Averaged  $\text{HCO}_3^-$  conductance with the control, ATP alone ( $n = 13$ ,  $*P < 0.05$ ), or ATP + cAMP ( $n = 4$ ). **c** Macroscopic  $I$ - $V$  relationships obtained in the presence of extracellular CFTRinh-172 at  $20 \mu\text{M}$  along with the standard NMDG-Cl pipette solution. **d** Averaged  $\text{HCO}_3^-$  conductance with the control, ATP alone, or ATP + cAMP ( $n = 11$ )

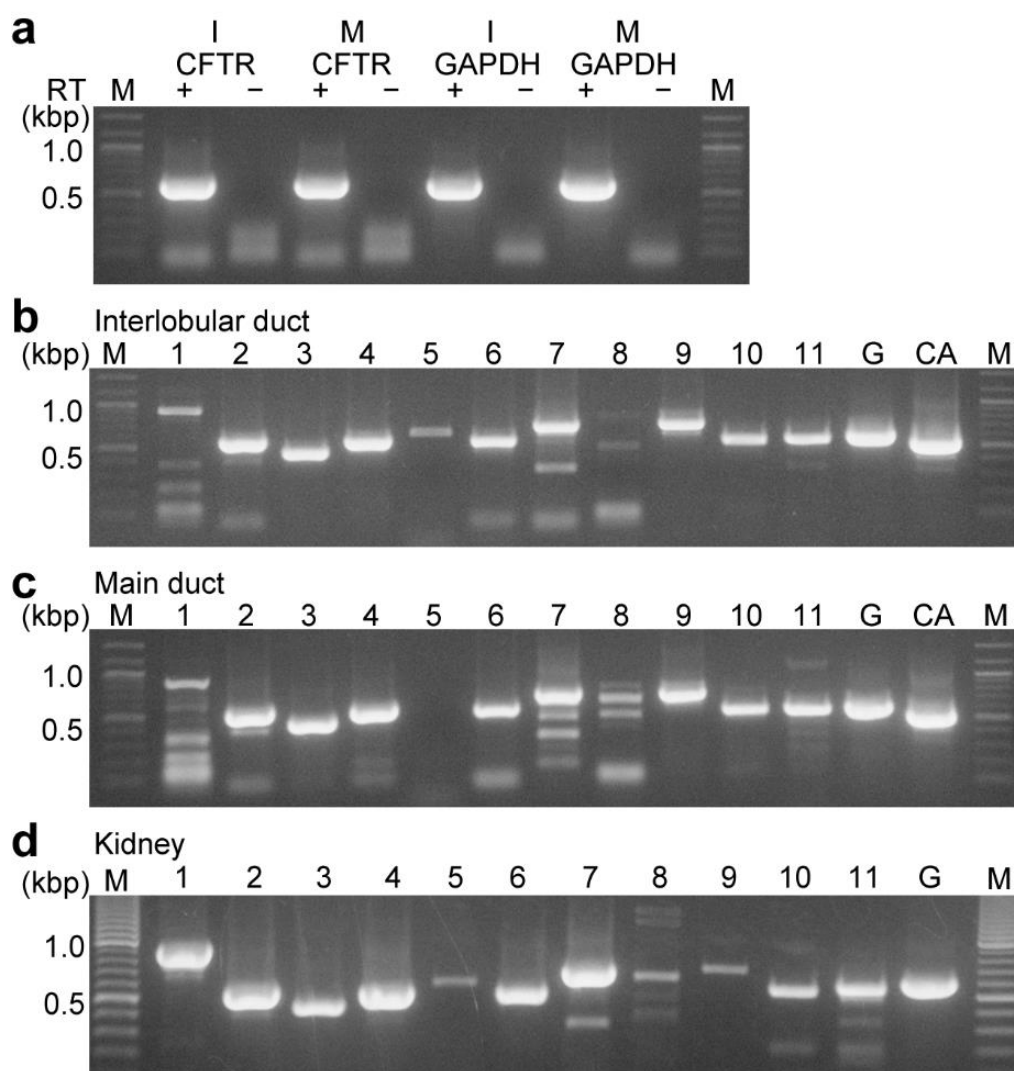


**Fig. 6** RT-PCR analysis of the SLC26A family. Ethidium bromide-stained agarose gels show RT-PCR products generated from total RNA isolated from the interlobular (I) and main (M) pancreatic ducts. **a** Control experiment shows the amplification of *Cftr* (623 bp) and *Gapdh* (610 bp). No DNA fragment was amplified with the template without reverse transcription (RT). The primers for the RT-PCR analysis from the interlobular (**b**) and main (**c**) ducts gave the expected fragment length for *Slc26a1-11* (Table 1). **d** Positive control obtained from the kidney. A representative gel for at least three independent experiments is shown. M in **a-d**: molecular mass, G in **b-d**: GAPDH, CA in **b** and **c**: carbonic anhydrase II

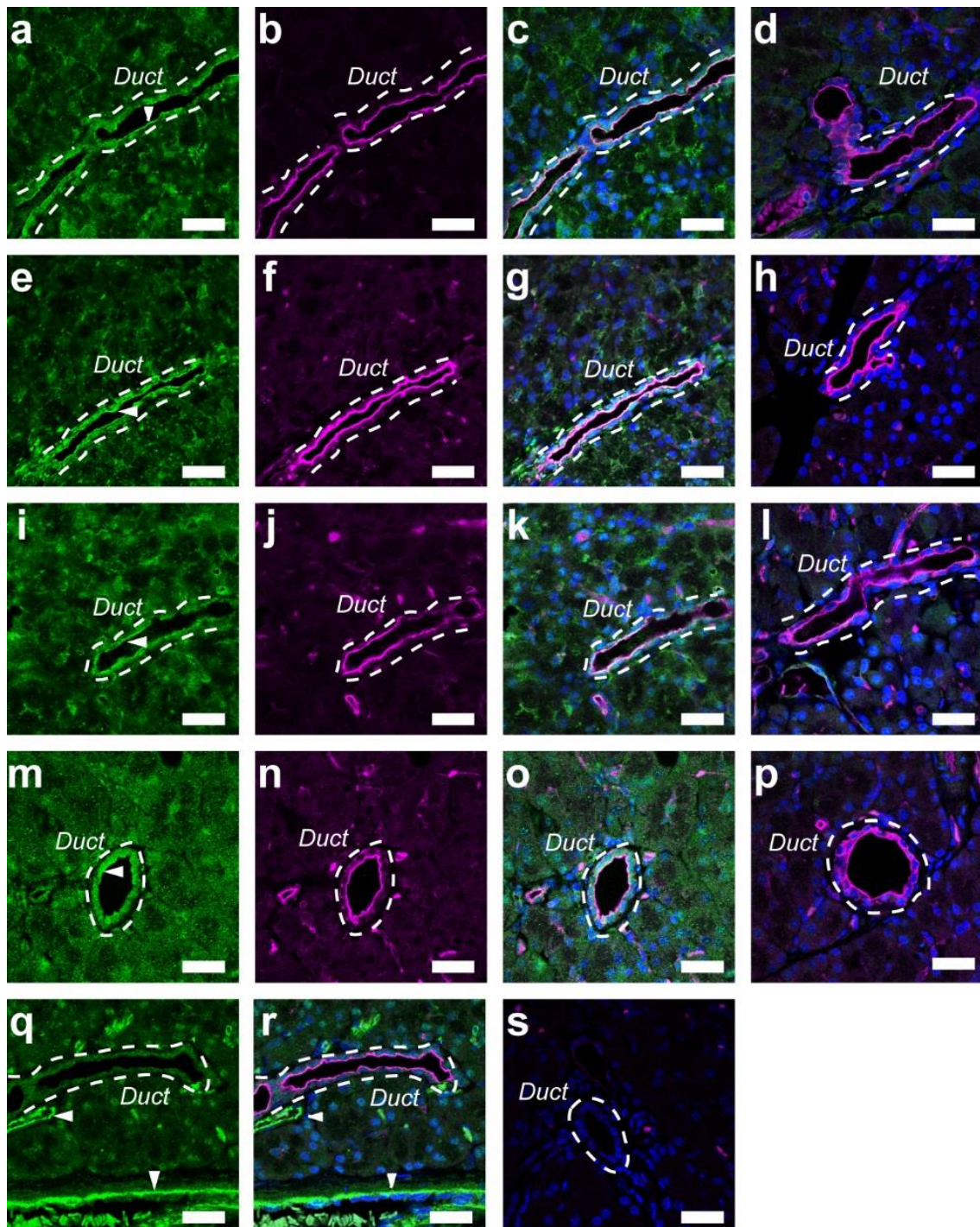


**Fig.7** Immunolocalization of the SLC26A family in the interlobular pancreatic duct. **a** Fluorescence of SLC26A6 on the luminal membranes of duct cells. **b** Fluorescence image of ezrin. **c** Overlay image of **a** and **b**. **d** Overlay image of ezrin and green fluorescence with SLC26A6 antibody pre-absorbed with the corresponding antigen.

The *broken line* indicates a duct. *Arrowhead* indicates the primary antibody signal on the luminal membrane. Fluorescence images of SLC26A1 (**e**), ezrin (**f**), overlay (**g**), and negative control with pre-absorbed SLC26A1 antibody (**h**). Fluorescence image of SLC26A4 (**i**), ezrin (**j**), overlay (**k**), and negative control with pre-absorbed SLC26A4 antibody (**l**). Fluorescence images of SLC26A10 (**m**), ezrin (**n**), overlay (**o**), and negative control with pre-absorbed SLC26A10 antibody (**p**). Fluorescence images of PECAM-1 (**q**), a blood vessel marker, and overlay with ezrin (**r**). *Arrowheads* show a blood vessel that does not overlap with the duct. **s** Control image of the guinea pig pancreas, in which primary antibodies were omitted. DAPI was used to stain nuclei (*blue*). Representative images for at least three independent experiments are shown.

*Bars* = 20  $\mu\text{m}$

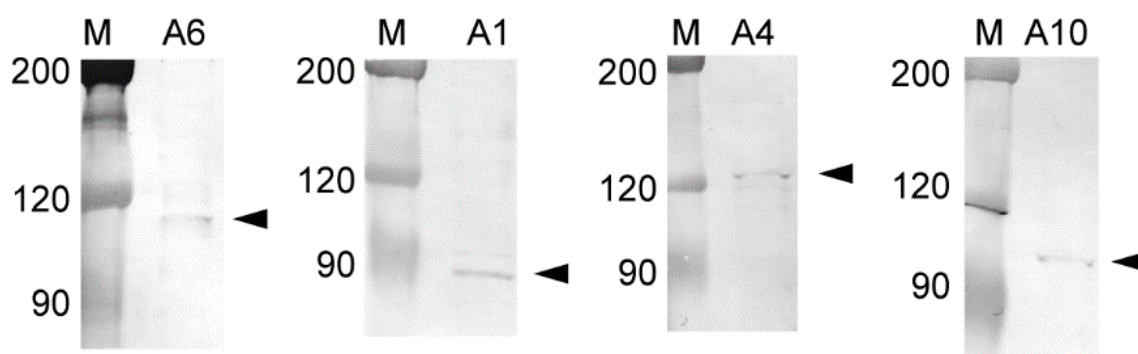


**Fig.8** Immunoblot of the SLC26A family from the pancreatic duct. Protein samples were resolved by SDS-PAGE. *Arrowheads* indicate SLC26A proteins detected by immunoblotting using anti-SLC26A antibodies. Representative membranes for at least three independent experiments are shown. M: marker, A6: SLC26A6, A1: SLC26A1, A4: SLC26A4, A10: SLC26A10

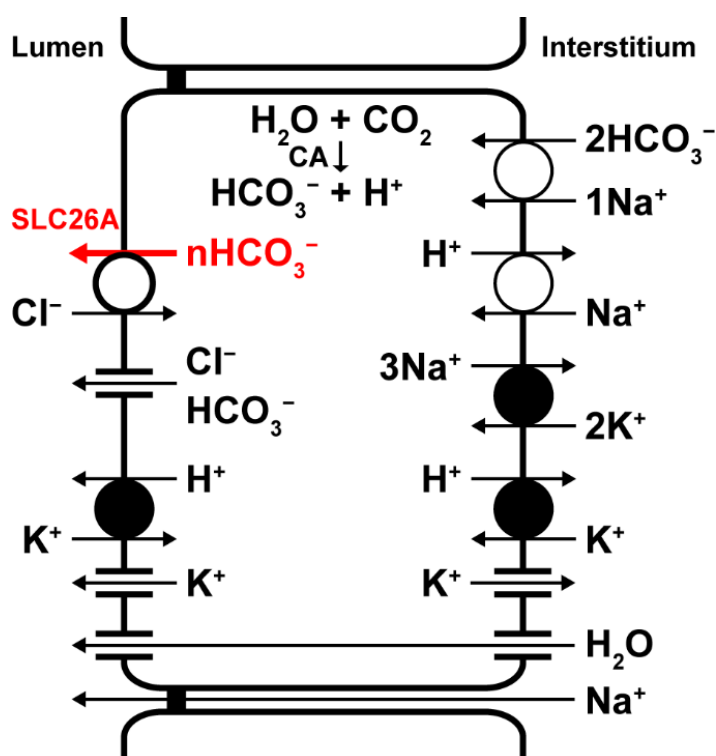


**Fig.9** Model of  $\text{HCO}_3^-$  transport in a pancreatic duct cell. Intracellular  $\text{HCO}_3^-$  is derived from  $\text{CO}_2$  through the action of carbonic anhydrase (CA) and from  $\text{HCO}_3^-$  uptake via the  $\text{Na}^+/\text{HCO}_3^-$  cotransporter.  $\text{H}^+$  is extruded at the basolateral membrane by the  $\text{Na}^+/\text{H}^+$  exchanger and  $\text{H}^+/\text{K}^+$  pump.  $\text{HCO}_3^-$  efflux across the luminal membrane is mediated by  $\text{Cl}^-$  channels (CFTR and TMEM16A/ANO1) and electrogenic  $\text{Cl}^-/n\text{HCO}_3^-$  exchangers (SLC26A1, 4, 6, and/or 10;  $n > 1$ ).  $\text{K}^+$  channels provide an exit pathway for  $\text{K}^+$  and play a vital role in maintaining the membrane potential, which is a crucial component of the driving force for anion secretion. Luminal  $\text{H}^+/\text{K}^+$  pumps may provide a buffering/protection zone for the alkali-secreting epithelium. Primary active transport is indicated by filled circles